https://doi.org/10.5194/wes-2025-263
Preprint. Discussion started: 21 January 2026

eawe european academy of wind energy
Open Access WIND ENERGY SCIENCE DISCUSSIONS

Aeroelastic Validation of ExaWind for the Pazy Wing Wind Tunnel Experiment

Neil Matula[1], Gopal Yalla[1], Bumseok Lee[3], Ganesh Vijayakumar[3], Nathaniel deVelder[2], Lawrence Cheung[2], Michael Sprague[3], and Paul Crozier[1]

[1]Sandia National Laboratories, Albuquerque, NM, USA
[2]Sandia National Laboratories, Livermore, CA, USA
[3]National Renewable Energy Laboratories, Golden, CO, USA

Correspondence: Neil Matula (nmatula@sandia.gov)

Abstract. This paper presents the results of a validation campaign of the fluid-structure interaction capability of the ExaWind software suite using the Pazy wing case, an aeroelastic benchmark featuring large nonlinear deformations of a very flexible wing under low-speed conditions. The simulations used the incompressible Reynolds-averaged Navier–Stokes equations equipped with a Shear-Stress Transport turbulence model for the fluid dynamics, together with a geometrically exact nonlinear beam model for the structural dynamics. The simulations yielded predictions of pre-flutter static deflections and flutter onset speeds that demonstrated strong agreement with both wind-tunnel data and the computational results contributed to the Large Deflection Working Group of the 3rd Aeroelastic Prediction Workshop.

1 Introduction

The future of wind energy depends strongly on the ability to predict the complex interactions between the structural dynamics of turbine blades and the surrounding turbulent flow of the atmospheric boundary layer. The current trend toward increasingly large and flexible turbine blades (Veers et al., 2003) drives the need for fluid-structure interaction (FSI) simulation software that can predict large, nonlinear deformations. It is equally important that these codes have strong credibility evidence to allow engineers to confidently explore this new design space.

The ExaWind software stack (Sprague et al., 2020; Sharma et al., 2024) is an open-source suite of high-fidelity computational physics codes for predictive simulations of wind turbines and farms, including software for computational fluid dynamics (CFD), structural dynamics (SD), environmental conditions, turbine control, and power generation. For blade-resolved FSI simulations, the primary codes in the ExaWind stack are Nalu-Wind (Sharma et al., 2024) , AMR-Wind (Kuhn et al., 2025), and OpenFAST (Jonkman et al., 2025); Nalu-Wind and AMR-Wind are coupled with the Topology Independent Overset Grid Assembler (TIOGA). While the individual codes in the ExaWind stack have been verified and validated in isolation, there is

https://doi.org/10.5194/wes-2025-263
Preprint. Discussion started: 21 January 2026

eawe european academy of wind energy
Open Access WIND ENERGY SCIENCE DISCUSSIONS

a need for credibility evidence for the coupled FSI solver. However, verification of the ExaWind FSI capability is nontrivial, as there are no available exact solutions that would fully exercise the solver capabilities, and the application of the method of manufactured solutions to coupled FSI solvers is a developing area of research. Hence, the bulk of the credibility evidence for coupled FSI codes must come in the form of experimental validation.

There are few examples of aeroelastic validation data for highly flexible wings at low speed conditions in the open literature. Tang and Dowell (2001) performed wind tunnel tests of a simple wing with a high aspect ratio at low speeds, but the deformations were relatively mild ($\sim 20\%$ span). Britt et al. (2012) tested a wing that underwent large relative deformations ($\sim 40\%$ span); however, the wing possesses significant additional surface complexity that is unsuitable for a validation case for wind turbine FSI codes. Cooper et al. (2019) tested a very flexible wing, but the test data and full details of the model are not openly available. The Pazy wing (Avin et al., 2022), on the other hand, is a low-speed benchmark that has a simple geometry suitable for code validation, undergoes large nonlinear deformations ($\sim 50\%$ span), and has extensive test data and simulation results available for comparison. The primary drawback of the Pazy wing in this context is that the wing aspect ratio (5.5) and size (0.55 meter span) are much smaller than that of a typical wind turbine blade. Nevertheless, because of the aforementioned advantages, we believe this experiment presents an excellent dataset for the validation of low-speed FSI codes at large relative deflections.

This paper presents the results of a validation campaign for the FSI capability of the ExaWind software stack using the Pazy wing benchmark. Predictions of pre-flutter static deflections and flutter onset speeds are compared against wind-tunnel data as well as computational results from the Large Deflection Working Group of the 3rd Aeroelastic Prediction Workshop (AePW3). This paper is structured as follows. Section 2 describes the components of the ExaWind suite used in this work. Section 3 describes the case details, mesh construction, model and solver parameters, and simulation results. Finally, we summarize our work in Section 4.

2 Models and Software

The ExaWind software suite is a collection of computational physics codes created to provide high-fidelity, predictive simulations that can be used to understand the complex multiscale, multiphysics of wind turbines and to create and test new engineering models. ExaWind was designed to be performance portable on modern high-performance-computing systems, and capable of running on both traditional CPU-based systems and those accelerated by graphical-processing units (GPUs) from multiple vendors. The ExaWind suite includes software for aerodynamics, structural dynamics, and code coupling, as well as supporting libraries. This section describes the elements of the ExaWind suite that are used in this work.

2.1 Nalu-Wind

Nalu-Wind (Sharma et al., 2024) is a wind-specific fork of the Nalu (Domino, 2015) low-speed CFD code. Nalu-Wind solves a finite-volume formulation of the accoustically incompressible Navier-Stokes equations using an unstructured-grid discretization, using an approximate pressure projection to enforce mass conservation. Options for modeling turbulent flows include

https://doi.org/10.5194/wes-2025-263
Preprint. Discussion started: 21 January 2026

Reynolds-averaged Navier-Stokes (RANS), large-eddy simulation (LES), and detached-eddy simulation (DES) models, together with a variety of options for subgrid-scale models. The temporal discretization uses either a first- or second-order backward-differentiation formula (BDF), which yields a coupled system of nonlinear algebraic equations that must be solved at every timestep. This system is solved using a segregated Picard iteration, together with a linear pressure-Poisson equation. The resulting linear systems are solved using the Krylov solver implementations and preconditioners provided by the Trilinos (Heroux et al., 2005) and *hypre* (Falgout and Yang, 2002) libraries. In particular, the algebraic multigrid preconditioners of the *hypre* library are frequently employed in blade resolved simulations, and indeed are essential for the performance of the pressure-Poisson solve. Nalu-Wind is written in C++ using modern software development practices, and has been shown to be performant on HPC systems (Mullowney et al., 2021). A more complete description of Nalu-Wind, including details of the temporal and spatial discretization, may be found in Sharma et al. (2024).

2.2 AMR-Wind

AMR-Wind (Kuhn et al., 2025) is an open-source incompressible flow solver develeped for wind turbine and farm simulations. AMR-Wind is massively parallel, and capable of utilizing GPU architectures. Built using the AMReX library, AMR-Wind allows adaptive or static mesh refinement of block-structured grids. It is capable of RANS and LES simulations, and is equipped with several subgrid-scale models. AMR-Wind is used to perform stand-alone simulations of turbulent atmospheric boundary layer (ABL) flows, and can also serve as a background solver for Nalu-Wind in blade-resolved turbine simulations. A more complete description of AMR-Wind may be found in Kuhn et al. (2025).

2.3 OpenFAST

OpenFAST[1] (Jonkman et al., 2025) is an open-source multiphysics code for the simulation of entire wind turbines. Developing from FAST version 8 (Jonkman, 2013), OpenFAST aims to couple together cost-effective models for all physical phenomena relevant to the design of wind turbines, including modules for aerodynamics/hydrodynamics, structural dynamics, environmental excitations (such as incoming wind and ocean waves), turbine control, and power generation and transmission.

OpenFAST is primarily used for time-domain simulations of entire turbines on ordinary personal computers to facilitate tight iteration loops in design. Hence, it employs low- and medium-fidelity engineering models for each turbine physics module, such as blade-element-momentum theory for the aerodynamics (AeroDyn) and nonlinear geometrically exact beam theory for the structural dynamics (BeamDyn (Wang et al., 2017)). However, the ExaWind framework permits coupling of the OpenFAST physics modules with high-fidelity simulation codes. In particular, CFD codes such as Nalu-Wind and AMR-Wind are frequently coupled together with BeamDyn to yield geometry-resolved fluid-structure interaction simulations.

[1] https://github.com/openfast/openfast

https://doi.org/10.5194/wes-2025-263
Preprint. Discussion started: 21 January 2026

eawe european academy of wind energy
Open Access WIND ENERGY SCIENCE DISCUSSIONS

2.4 Coupled FSI Simulations using ExaWind

The structured nature of the AMR-Wind code, together with its mesh refinement capability, makes it very cost-effective for accurately simulating turbulent flows within simple, "box-shapped" domains, such as an ABL over flat terrain. However, it cannot utilize body-fitted grids, and is therefore not well-suited to blade-resolved simulations, where satisfactory resolution of the blade boundary layer and immediate wake are of paramount importance. Nalu-Wind, on the other hand, can effectively handle the flow around the turbine using body-fitted grids, but its unstructured-grid algorithm makes it less efficient in capturing the farfield flow. The strengths of each code suggest a natural strategy: Nalu-Wind may be used to simulate the flow near the turbine using a body-fitted computational grid, while the farfield can be handled by AMR-Wind using its structured-grid approach with mesh refinement. At the interface between the two subdomains, an overset ("chimera") approach is employed using the TIOGA[2] library (Roget and Sitaraman, 2014; Brazell et al., 2016). Detailed descriptions of the overset coupling and solution scheme may be found in papers by Sharma et al. (2024, 2021).

For FSI simulations of horizontal-axis wind turbines using ExaWind, the blade and tower deformations are typically computed by the structural dynamics modules of OpenFAST. The blades and tower each have one spatial dimension that is much larger than the others, and hence may be reasonably approximated as beams; the BeamDyn module of OpenFAST is therefore appropriate. At each timestep, the aerodynamic loads from Nalu-Wind are sent to OpenFAST, and the displacements from OpenFAST are sent to Nalu-Wind. The overall residuals are not typically iterated to convergence; that is, BeamDyn and the CFD codes are each only called once per timestep. While the ExaWind driver provides the option of using multiple outer Picard iterations to converge the solutions Nalu-Wind and OpenFAST together, a single Picard iteration is most commonly used.

3 Pazy Wing FSI Simulations

3.1 Case Description

The Pazy wing experiment was designed to provide a low-speed aeroelastic benchmark case in the open literature for validation of FSI simulation software. The nominal design geometry is a straight wing with a uniform NACA0018 airfoil section along the span. While the design specifications call for a clean wing with no sweep, twist, or taper, the as-built geometry used in the wind-tunnel experiments contained small deviations from the nominal shape, including flapwise bend, approximately 1 degree of twist, and sagging of the wing surface between the structural ribs. These deviations are expected to have a small impact on the results, and are neglected in the present analysis. Additionally, the experiments used a weight mounted on the tip of the wing to control the flutter boundaries. The simulations in this work included the effect of the weight as a point mass in the structural model, but the shape of the weight was not included in the CFD model.

The experiments were performed in a low-speed wind tunnel in the incompressible regime. The wing was mounted vertically from the floor of the wind tunnel, which reduced (but did not completely eliminate) the impact of gravity on the wing deformations. The density and molecular viscosity corresponded to standard atmospheric conditions, the wind speed varied

[2]https://github.com/ExaWind/tioga

https://doi.org/10.5194/wes-2025-263
Preprint. Discussion started: 21 January 2026

eawe european academy of wind energy
Open Access WIND ENERGY SCIENCE DISCUSSIONS

Wing geometry	
Span	0.55 m
Chord	0.10 m
Airfoil	NACA0018
Root AoA	$\in [3, 7]$ degrees
Freestream conditions	
Dynamic viscosity	1.8×10^{-5} Pa s
Density	1.225 kg m^{-3}
Velocity	$\in [15, 50]$ m s^{-1}
Mach number	$\in [0.04, 0.15]$
Reynolds number	$\in [1.0, 3.4] \times 10^5$
Turbulence intensity	0.5%

Table 1. Summary of the geometry and flow conditions of the Pazy wing experiment (Avin et al., 2022).

from 15 to 50 m s^{-1}, and the root angle of attack (AoA) of the wing ranged from 3–7 degrees. A summary of the geometry and flow conditions is shown in Table 1, and a complete description of the tests is provided by Avin et al. (2022).

Two datasets from the original Pazy wing experiments are used for comparison in this work. First, the wing was subjected to pre-flutter wind conditions, and static deflection measurements were collected for varying wind speeds and angles of attack, which will be the primary quantity of interest (QoI) for our analysis using this first dataset. Second, the wing was subjected to higher wind speeds that yielded vibrational instabilities. The primary QoI for this second set of tests will be the flutter onset speed as a function of the angle of attack.

3.2 Mesh Generation

The CFD computational domain is illustrated in Figure 1. The air flow enters the domain at the boundary marked “Inlet”, and exits at the boundary marked “Outlet”. The boundaries marked “Slip Wall” represent the sides, ceiling, and floor of the wind tunnel. The use of zero-velocity boundary conditions (“no-slip”) on these walls would yield a higher fidelity calculation by capturing the effect of the boundary layers attached to the wind tunnel walls. However, it is expected that these boundary layers have a minimal influence on the aeroelastic behavior of the wing, and hence no-penetration boundary conditions were used here instead to reduce simulation cost. The wing surface, marked “No-Slip Wall”, uses a zero-velocity boundary condition. Finally, the surface marked “Overset” denotes the interface between the Nalu-Wind and AMR-Wind domains. Since overset interpolation is used during the coupled CFD simulations, the Nalu-Wind and AMR-Wind meshes may be generated independently, with the only constraint being that the cells of both domains near the interface should be of similar sizes and aspect ratios, and in fact, should ideally approximate cubes.

https://doi.org/10.5194/wes-2025-263
Preprint. Discussion started: 21 January 2026

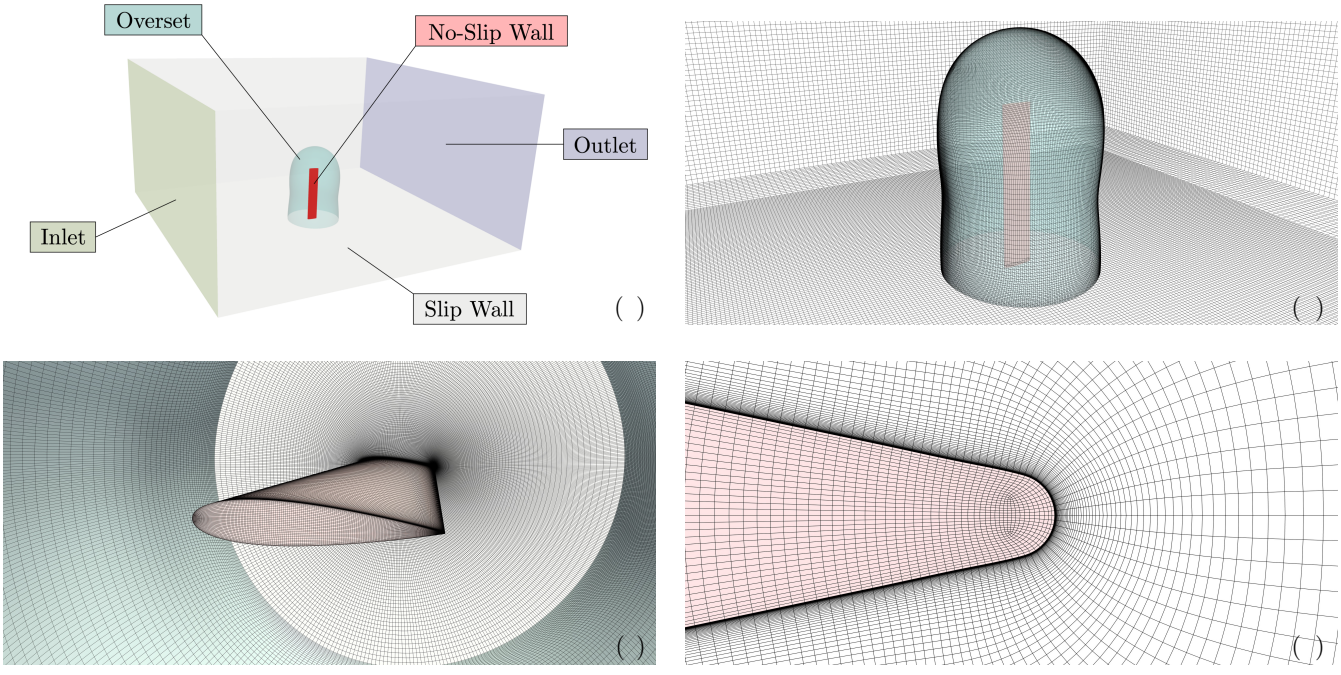

Figure 1. (a) Computational domain and boundary conditions, (b) overview of baseline meshes for Nalu-Wind (cyan and red) and AMR-Wind (grey), (c) span-wise view of the baseline Nalu-Wind mesh boundary surfaces, and (d) detailed view of the trailing edge of the baseline Nalu-Wind mesh: O-H "butterfly" (red) on the wing tip, and root slice of the volume grid (grey).

AMR-Wind uses a cartesian mesh composed of cube cells, which is locally refined in either a static or adaptive fashion. For this work, a single static refinement zone in the shape of a rectangular prism is nested inside the base level. Each refinement level divides the elements of the previous level into 8 child elements. This approach creates a graded mesh between the farfield and near-body region, allowing the AMR-Wind and Nalu-Wind meshes to have similar element sizes at the overset interface.

The Nalu-Wind mesh is generated using the commercial software Pointwise (Cadence Design Systems). The surface of the wing is meshed in two parts: the tip airfoil, and the lifting surface. As mentioned in the Case Description section above, the experimental model included a weight mounted on the tip of the wing. Since the effect of the weight is neglected in the CFD portion of the analysis, the wing was instead simply truncated at the tip with a flat airfoil section. The tip airfoil is meshed using an O-H ("butterfly") topology, and the O- and H-blocks are smoothed together using the elliptic solver provided in PointWise. The mesh for the lifting surface is then formed from a direct extrusion of the airfoil point distribution. The volume mesh is obtained by a hyperbolic extrusion of the multi-block surface mesh, resulting in an O-type topology along the lifting surface.

This approach allows for elements near the overset interface that are approximately cubes, which improves the quality of the overset interpolation between the AMR-Wind mesh and the Nalu-Wind mesh. Because the NACA0018 airfoil section nominally has a sharp trailing edge, a C-type mesh would perhaps be more natural than an O-type mesh for the volume mesh. However, a C-type mesh would yield elements with dramatically varying sizes and aspect ratios at the overset boundary,

https://doi.org/10.5194/wes-2025-263
Preprint. Discussion started: 21 January 2026

eawe european academy of wind energy
Open Access WIND ENERGY SCIENCE DISCUSSIONS

AMR-Wind mesh	
Domain size	3 m × 3 m × 1.5 m
Level 0 dimensions	128 × 128 × 64
Level 0 spacing	0.024 m (24% chord)
Level 1 spacing	0.012 m (12% chord)
Total cell count	5,767,168
Nalu-Wind mesh	
First cell height	1.0×10^{-6} m
First cell y^+	0.2
Initial growth rate	1.1
Total normal distance	0.2 m (200% chord)
Normal cell count	150
Airfoil cell count	500
Spanwise cell count	100
Total cell count	8,736,600

Table 2. Parameters of the baseline CFD meshes. For the AMR-Wind domain size and dimensions, the first value corresponds to the streamwise direction, the second value corresponds to the lateral direction, and the final value to the spanwise direction. Note that the AMR-Wind cell count includes cells from all refinement levels, and the total normal distance for the Nalu-Wind mesh is approximate, as it varies around the airfoil circumference.

resulting in poor interpolation quality. Hence, an O-type extrusion is typically used for the volume mesh in blade-resolved ExaWind simulations, and this approach is used here. The tradeoff is that a small amount of trailing edge rounding was required to obtain a satisfactory mesh extrusion, resulting in a chord length that is approximately 3% less than the nominal value. However, this deviation is expected to have a negligible impact on the results.

In the wind tunnel experiment, the lateral dimension (across the test section) is small enough that the wing tip would pass near the walls at maximum deflection. This would yield potential difficulties with the O-type extrusion of the blade mesh at the tip, as it could pass through the side wall boundaries at maximum deflection. For this reason, the lateral dimension of the wind tunnel was enlarged somewhat to ensure no collisions could occur. The other dimensions of the AMR-Wind domain were selected somewhat arbitrarily, with only the requirement that the boundaries are placed at least 10 chord lengths away from the object to avoid contamination from the numerical boundary conditions. The baseline meshes for AMR-Wind and Nalu-Wind are shown in Figure 1, and selected details of the baseline meshes are shown in Table 2.

https://doi.org/10.5194/wes-2025-263
Preprint. Discussion started: 21 January 2026

eawe european academy of wind energy
Open Access WIND ENERGY SCIENCE DISCUSSIONS

3.3 Model and Solver Parameters

Spectral data from the wind tunnel experiments suggested that while the primary flutter mode was excited at around 28 Hz (corresponding to the natural frequency of the first torsion mode), important contributions were observed at 80 Hz (corresponding to the third bending mode). To estimate a sufficiently small simulation timestep, we applied a simple heuristic of requiring at least 100 samples per period of the third bending mode, leading to a timestep of $\Delta t \approx 1.0 \times 10^{-4}$ s. For the CFD contribution, the baseline grid above resulted in the AMR-Wind stability criterion being the ultimate limiting factor, which led to a timestep limit of approximately 6.0×10^{-5} s at the highest wind speeds. This fortuitously was close to the aforementioned accuracy requirement. Hence, a value of 6.0×10^{-5} s was selected for the baseline CFD timestep. The time-stepping algorithm for the ExaWind FSI capability requires that the CFD timestep be an integer multiple of the SD timestep, such that all codes synchronize at every CFD timestep. Naturally, the total computational cost of an OpenFAST/BeamDyn step is miniscule compared to that of a CFD step. However, OpenFAST is currently not parallelized, while the CFD solvers are. As a result, while the wallclock time needed to complete an SD step is indeed much less than that of a CFD step, it is not entirely negligible. Practical experience with the ExaWind FSI capability has led to a standard practice of $\mathcal{O}(10)$ SD steps for every CFD step. Since the timestep size needed for stability of the CFD calculation was already quite close to a conservative estimate of the accuracy requirement for the SD step, a (somewhat arbitrary) value of 3:1 was selected for the ratio of CFD to SD timesteps, leading to a baseline timestep of 2.0×10^{-6} s for OpenFAST/BeamDyn. Although these choices for the CFD and SD timesteps were dictated by the highest wind speed, for simplicity they are used across all wind speeds.

The CFD simulations were performed in RANS mode using the 2003 formulation of Menter's k–ω SST turbulence model (Menter et al., 2003) in both AMR-Wind and Nalu-Wind, coupled together with the one-equation γ-model for transition introduced by Menter et al. (2015). Because the inlet of the CFD domain is a substantial distance from the wing, it is expected that without intervention, the inlet turbulence level will have decayed by the time the flow reaches the wing. Using a method introduced by Lee et al. (2025), the local turbulence intensity is instead specified everywhere in the domain to be equal to the intensity measured in the wind-tunnel experiments. This approach allows the turbulence intensity to be sustained in a manner that is compatible with the transition model. A variant of the Weighted Essentially Nonoscillatory scheme, known as WENO-Z (Borges et al., 2008), was used for the advection scheme in AMR-Wind. While variable-density simulations are possible using the ExaWind suite, the calculations here used a fully incompressible fluid with constant density. The flow was initialized using a "plug flow" (i.e. constant velocity) condition, with all quantities set to the inlet values. Nalu-Wind used 4 internal Picard iterations for each timestep, but no outer loops were used between the codes.

The SD simulations used a single 9^{th} order Legendre spectral finite element for the wing, and zero deflection and applied aerodynamic loads were provided on initialization. The sectional properties of the beam model were taken from the UM/NAST nonlinear beam model (Riso and Cesnik, 2023a, b), which was used in the AePW3. Stiffness-proportional damping is incorporated in the structural model, with a constant value of $\mu = 10^{-6}$ used for all 6 degrees of freedom. Numerical damping is also included in the time-stepping scheme through the use of a generalized-α integrator, for which maximum numerical damping was prescribed. Because of the vertical orientation of the wing, the effect of gravity was initially presumed to be negligible, and

https://doi.org/10.5194/wes-2025-263
Preprint. Discussion started: 21 January 2026

eawe european academy of wind energy
Open Access WIND ENERGY SCIENCE DISCUSSIONS

our early simulations did not provide a gravity source. This led to an initial underprediction of the tip deflection, and subsequent testing revealed that the effect of gravity on the wing behavior was, in fact, significant. Hence, a gravitational acceleration of $9.81\ \mathrm{m\ s^{-2}}$ was ultimately used in the structural calculations. No gravity was included in the CFD calculations, however.

3.4 Simulation Methodology and Determination of Flutter Onset

As mentioned in the previous section, the simulations were performed from a "cold start"; that is, AMR-Wind and Nalu-Wind began the simulation with a uniform initial flowfield, and BeamDyn/OpenFAST began the simulation with zero deformation and applied aerodynamic loads. Alternative initialization approaches are possible. For example, the user could begin with a CFD-only simulation to establish the basic flow, and then incorporate the deflections from OpenFAST/BeamDyn by slowly ramping to their full value. This approach would minimize the numerical difficulties associated with initial transients, at the expense of additional compute resources. However, the cold-start approach yields the added benefit of demonstrating the robustness of the coupled FSI solver.

Simulations were performed at individual wind speed and AoA pairs. It should be noted that the static deflection and flutter simulations use the same simulation parameters (grid, models, discretization, numerics, damping, etc.), and as a consequence, the ultimate behavior (steady state versus flutter) is only determined by the freestream wind speed and root AoA of the wing. Each simulation was nominally carried out for 2.5 seconds, which was found to be sufficient to observe the long-time behavior of the system. Since the simulations begin with the wing in an undeformed state, initial transient behavior is observed in the time history of the tip deflection. For wind speeds well below the flutter onset boundary, these initial transients decay, and the tip deflection approaches a clear steady state. For wind speeds well above the flutter onset boundary (but well below the offset boundary), the oscillations in the tip deflection grow in magnitude, apparently without bound, and eventually lead to solver failure. (This was not deemed concerning, because as the instabilities continue to grow, the elastic structural model is eventually no longer applicable, and the simulation enters an unphysical state.) Hence, it is easy to identify conditions that are clearly stable, and those that clearly demonstrate flutter. However, determining the exact location at which the instabilities begin to grow without bound is difficult, and the result would likely be sensitive to the initial conditions, as well as model and solver parameters. Instead, a bracketing approach is used, wherein simulations were performed using a range of wind speeds that brackets the experimental onset boundary, and each speed was placed in one of three categories according to the qualitative behavior of the tip deflection history:

1. *Stable* – the initial transients decay, and the deflection reaches a clear steady state,
2. *Unstable* – the large initial transients decay, but smaller oscillations persist with no apparent end, and
3. *Flutter* – the transients do not decay, and instead increase, apparently without bound.

A representative example of these three categories is shown in Fig. 2 for a root AoA of 7°. In this manner, the flutter onset boundary can confidently be said to be between the "Stable" and "Flutter" conditions. If a more precise estimate is required, the "Unstable" condition may be used to approximate the flutter onset speed, although not with the same degree of confidence because, as mentioned above, the behavior of the simulation at this speed will likely be sensitive to model and solver parameters.

https://doi.org/10.5194/wes-2025-263
Preprint. Discussion started: 21 January 2026

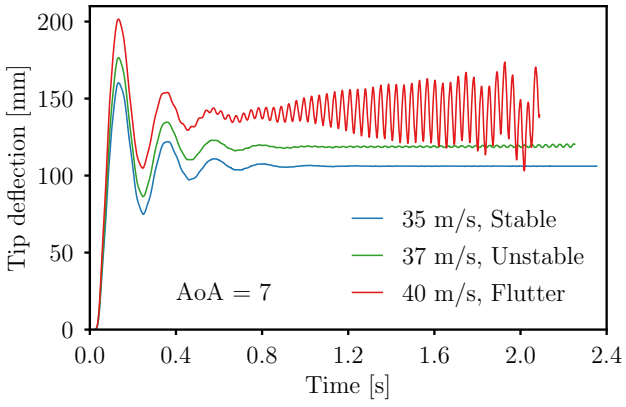

Figure 2. Time history of flap-wise tip deflection for a root AoA of 7° at three windspeeds near the flutter onset boundary.

It should be noted that there exist other possible ways to structure the simulations for detecting the flutter onset speed. For example, rather than performing simulations at different wind speeds, one could instead perform one simulation with a time-dependent freestream velocity that slowly sweeps through the desired range of wind speeds. This would have the advantage of more closely resembling the actual wind tunnel tests. However, this approach would have the drawback of introducing a dependence on the direction and rate of the sweep; indeed, the wind tunnel data showed that low-to-high sweeps produced a different result than high-to-low sweeps. Furthermore, this approach would limit the parallelizability of the simulations, requiring very long jobs with many restarts rather than many jobs in parallel. For these reasons, individual simulations at constant bracketing wind speeds were chosen for this work.

3.5 Software Versions and Code Performance

The simulation results presented here may be reproduced using the following code commits:

ExaWind Driver:	`046b080c7e0f0ab1efea0dccb4f798fe84ef905e`
Nalu-Wind:	`b9e4ae654b646ecd0501dd6391dc7537239c82db`
AMR-Wind:	`b61c01895e8eab388e4a3fd129e1db0f4fd0f534`
OpenFAST:	`024dbc1816ca8caeefcc720b1099397730b1ec0a`

The simulations were run on HPC systems at Sandia National Laboratories. A typical simulation was performed using 560 CPUs across 5 HPC nodes. Each simulation used approximately 48 wallclock hours to yield approximately 2 seconds of simulated time.

https://doi.org/10.5194/wes-2025-263
Preprint. Discussion started: 21 January 2026

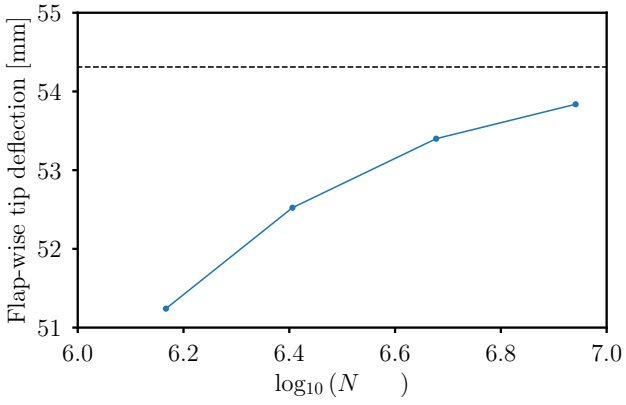

Figure 3. Steady-state flap-wise tip deflection versus mesh size for a root AoA of 7° and wind speed of 25 m s^{-1}. The solid blue line indicates the simulation results, and the dashed black line indicates the estimated continuum value based on a Richardson extrapolation of the simulation results. The horizontal axis is a measure of the number of grid cells in each coordinate direction, and N_{elem} is the number of elements in the Nalu-Wind mesh. (The AMR-Wind mesh is refined together at the same rate as the Nalu-Wind mesh.)

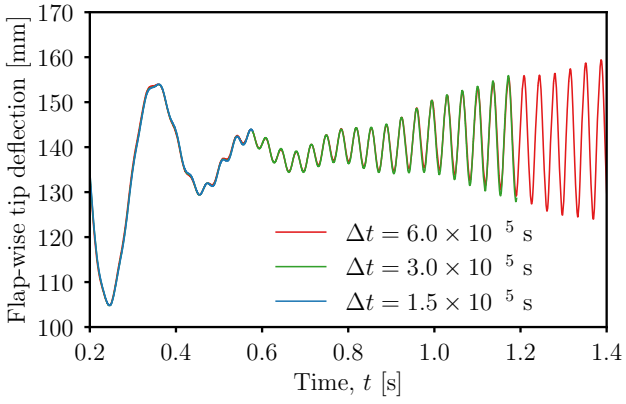

Figure 4. Flap-wise tip deflection history for a root AoA of 7° and wind speed of 40 m s^{-1} at three different timestep sizes.

3.6 Mesh and Timestep Refinement Studies

To determine the sensitivity of the results to the spatial resolution of the CFD mesh and timestep, two studies were conducted. The first was a static deflection case at an AoA of 7 degrees and wind speed of 25 m s^{-1}. Since AMR-Wind was operating near its stability limit at the baseline mesh resolution and timestep, in order to fix the timestep, it was necessary to *coarsen* the mesh from the baseline resolution, rather than refine it. The meshes are coarsened uniformly in each dimension, and the meshes for both AMR-Wind and Nalu-Wind are coarsened at the same rate, such that the cells at each side of the interface remain of a

https://doi.org/10.5194/wes-2025-263
Preprint. Discussion started: 21 January 2026

eawe european academy of wind energy
Open Access WIND ENERGY SCIENCE DISCUSSIONS

comparable size at each refinement level. The results of this study are shown in Figure 3, where the dashed line denotes an estimate of the continuum value of the tip deflection. This estimate was calculated using a Richardson extrapolation method of the form

$$f_h = f_{h=0} + Ah + Bh^2 + Ch^3,$$

where f_h is the tip deflection at a particular resolution h, $f_{h=0}$ is the continuum value of the tip deflection, and A, B, and C are constants independent of mesh resolution. The four constants ($f_{h=0}$, A, B, and C) were found by demanding that the model predict the simulated tip deflections for each of the four mesh resolutions. The results suggest that the baseline mesh is able to predict the tip deflection within 1% of the continuum value, thereby providing evidence that the mesh resolution is sufficient for this QoI. It should be stressed that while the horizontal axis of Figure 3 uses the number of cells in the Nalu-Wind mesh, the AMR-Wind mesh is coarsened proportionally, such that the ratio of element sizes across the mesh interface stays approximately constant.

The second study examined the impact of the timestep size while holding the mesh resolution constant. Figure 4 shows the history of tip deflection for three different CFD timestep sizes at a root AoA of 7° and wind speed of 40 m s^{-1}. Since AMR-Wind was operating near its stability limit on the baseline mesh, it was necessary to *refine* the timestep from the baseline value, rather than coarsen it. The CFD-to-SD timestep ratio was held at 3:1 for all simulations. The results qualitatively suggest that the baseline timestep is more than sufficient for the accuracy of these simulations.

3.7 Results: Static Deflection

Figure 5 presents the results of the simulations at sub-flutter wind speeds. Two different sets of results from the original experiments (Avin et al., 2022) are shown for comparison: one is a sweep of dynamic pressure q at a constant root AoA, and the other is a sweep of AoA at a constant dynamic pressure. The Pazy wing case was the focus of the Large Deflection Working Group of the 3$^{\text{rd}}$ Aeroelastic Prediction Workshop (Ritter et al., 2024), and the range of the computational results contributed for this workshop are denoted by the grey band, labeled "Workshop". Excellent agreement is observed between the present analysis and the experiment at all wind speeds and angles of attack, although better agreement is noted with q-sweep. The ExaWind results are also in good agreement with the computational results from the workshop, indicating that the relevant physical phenomena of the Pazy wing case can be adequately captured by a variety of simulation methodologies. It is worth noting that both the ExaWind and workshop results demonstrate better agreement with the q-sweep. Finally, it should be noted that the impact of the transition model varies with the AoA. At the lowest AoA (3 degrees), the results are practically identical with and without the transition model. At the intermediate AoA (5 degrees), the transition model arguably yields slightly worse agreement, although the discrepancy is small compared to the uncertainty of the measurements. At the highest AoA (7 degrees), however, the transition model yields significantly improved agreement.

https://doi.org/10.5194/wes-2025-263
Preprint. Discussion started: 21 January 2026

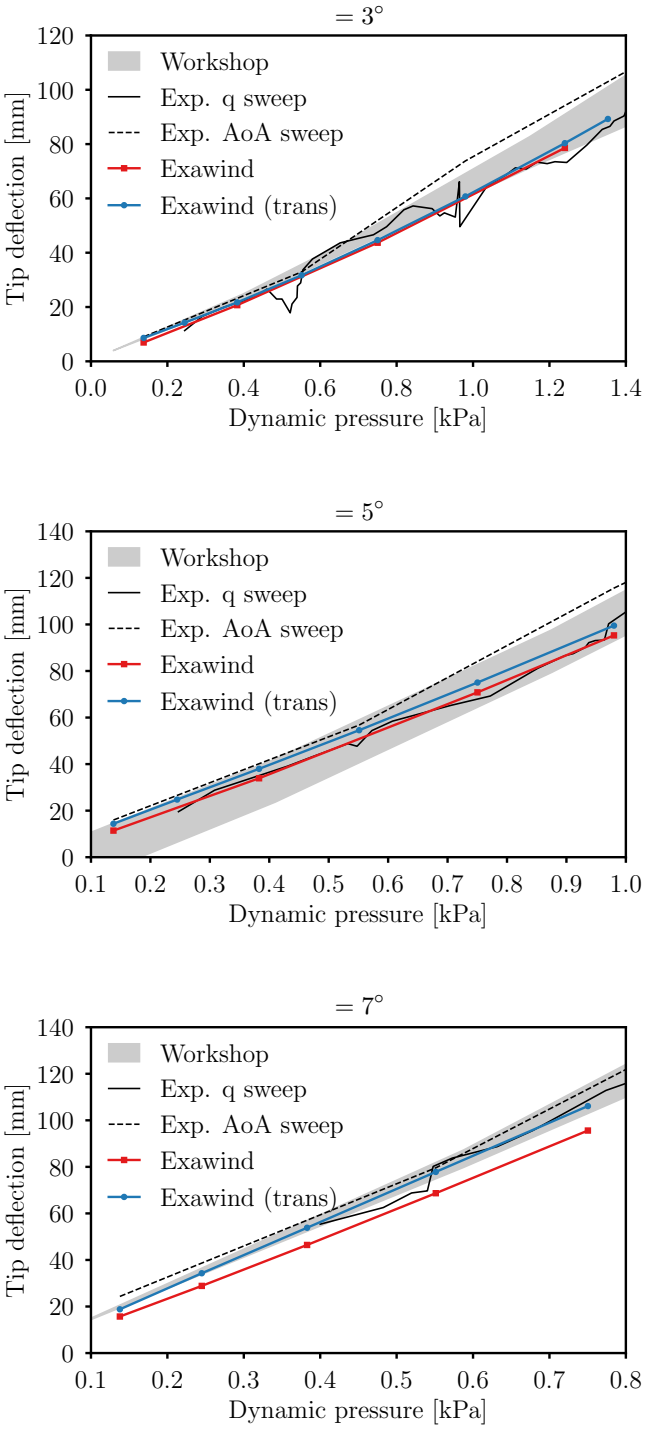

Figure 5. Static flap-wise tip deflection versus freestream wind speed for various angles of attack: comparison between wind-tunnel experiments, ExaWind simulation results, and the contributed simulation results for AePW3.

https://doi.org/10.5194/wes-2025-263
Preprint. Discussion started: 21 January 2026

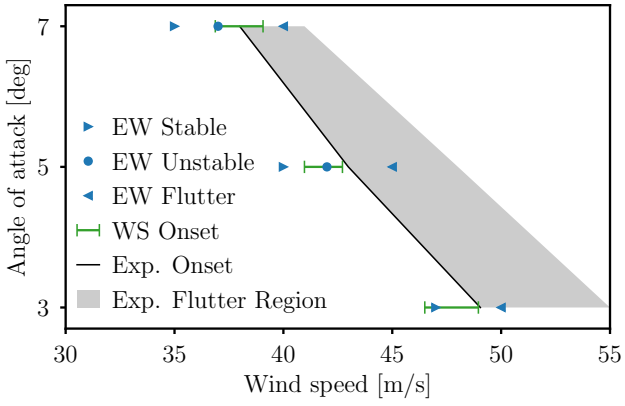

Figure 6. Flutter onset speed versus root AoA: comparison between wind-tunnel experiments, ExaWind simulation results, and the contributed simulation results for AePW3.

3.8 Results: Flutter Onset

Figure 6 presents the results of the simulations near the experimental flutter onset speed. Here, the grey region indicates the experimental instability region, the solid black line indicates the experimental onset speed, and the green interval indicates the range of simulation results for the onset speed contributed for the AeWP3. The ExaWind results are indicated by the blue symbols: The right-pointing triangles (labeled "Stable") denote conditions that clearly indicated a stable steady-state result, the left-pointing triangles (labeled "Flutter") denote conditions that clearly demonstrated flutter, and the circles (labeled "Unstable") denote conditions for which the simulated tip deflection did not approach a steady state, but also did not increase without bound.

As discussed above, the flutter onset speed prediction is characterized by the interval between the "Stable" and "Flutter" symbols at a given root AoA. The "Unstable" symbol can serve as a more precise estimate of the onset speed if needed. The results indicate that the experimental onset speed was successfully bracketed within $\pm 7\%$ of the experimental value. Further, the "Unstable" value is within about 3% of the experimental value, and agrees well with the predictions of the AeWP3. It should be noted that no "Unstable" condition was identified for an AoA of 3°. This occurred because three speeds were selected *a priori* near the flutter onset boundary for each AoA, and simulations for all sets of conditions were performed in parallel. While the 5° and 7° cases yielded one result in each of the three categories, it happened that the 3° cases did not yield an "Unstable" condition. However, the advantage of this result is that a tighter bracket was found for this AoA. Future studies are planned to tighten the flutter onset brackets at all angles of attack.

https://doi.org/10.5194/wes-2025-263
Preprint. Discussion started: 21 January 2026

eawe european academy of wind energy
Open Access WIND ENERGY SCIENCE DISCUSSIONS

4 Conclusions

In this paper, we presented the results of a validation campaign of the ExaWind FSI capability using the Pazy wing aeroelastic benchmark. The results were compared to those of the original wind-tunnel tests, as well as to the computational results contributed to the Large Deflection Working Group of the 3rd Aeroelastic Prediction Workshop. The ExaWind results show good agreement with both the experimental and computational comparison data, providing credibility evidence for the ExaWind FSI capability in the context of low-speed atmospheric flows and very flexible structures.

Author contributions. NM was responsible for model setup, meshing, parameter tuning, production simulations, post-processing, and paper preparation. GY assisted with checking the model setup and paper preparation. BL provided guidance for the setup of his transition model, and assisted with paper preparation. GV provided guidance on model setup and debugging, and assisted with paper preparation. ND, LC, MS, and PC provided technical guidance and feedback, and assisted with paper preparation.

Competing interests. The contact author has declared that none of the authors has any competing interests.

Acknowledgements. The authors would like to acknowledge members of the ExaWind and HFM teams and their contributions to the ExaWind software stack. The work was authored in part by Sandia National Laboratories, a multimission laboratory managed and operated by the National Technology and Engineering Solutions of Sandia, LLC (NTESS), a wholly owned subsidiary of Honeywell International Inc., for the US DOE's NNSA under contract no. DE-NA0003525. This work was also authored in part by NREL for the U.S. Department of Energy (DOE), operated under Contract No. DE-AC36-08GO28308. This research was supported by the DOE Office of Energy Efficiency and Renewable Energy Wind Energy Technologies Office. This research used high-performance computing resources located at Sandia National Laboratories. The views expressed in the article do not necessarily represent the views of the DOE or the US Government. The US Government retains and the publisher, by accepting the article for publication, acknowledges that the US Government retains a nonexclusive, paid-up, irrevocable, worldwide license to publish or reproduce the published form of this work, or allow others to do so, for US Government purposes.

https://doi.org/10.5194/wes-2025-263
Preprint. Discussion started: 21 January 2026

eawe european academy of wind energy
Open Access WIND ENERGY SCIENCE DISCUSSIONS

References

Avin, O., Raveh, D. E., Drachinsky, A., Ben-Shmuel, Y., and Tur, M.: Experimental aeroelastic benchmark of a very flexible wing, AIAA Journal, 60, 1745–1768, https://doi.org/10.2514/1.J060621, 2022.

Borges, R., Carmona, M., Costa, B., and Don, W. S.: An improved weighted essentially non-oscillatory scheme for hyperbolic conservation laws, Journal of Computational Physics, 227, 3191–3211, https://doi.org/10.1016/j.jcp.2007.11.038, 2008.

Brazell, M. J., Sitaraman, J., and Mavriplis, D. J.: An overset mesh approach for 3D mixed element high-order discretizations, Journal of Computational Physics, 322, 33–51, https://doi.org/10.1016/j.jcp.2016.06.031, 2016.

Britt, R., Ortega, D., Mc Tigue, J., and Scott, M.: Wind tunnel test of a very flexible aircraft wing, in: 53rd AIAA/ASME/ASCE/AHS/ASC Structures, Structural Dynamics and Materials Conference 20th AIAA/ASME/AHS Adaptive Structures Conference 14th AIAA, p. 1464, https://doi.org/10.2514/6.2012-1464, 2012.

Cadence Design Systems: Pointwise, https://www.cadence.com/en_US/home/tools/system-analysis/computational-fluid-dynamics/fidelity.html#fidelity-pointwise.

Cooper, J. E., Cook, R. G., Francois, G., Rodríguez, O., Neild, S. A., Lowenberg, M. H., Alexander, S. S., Coetzee, E. B., and Evans, M.: Wind tunnel testing of a high aspect ratio wing model, in: Proceedings of Forum of Aeroelasticity and Structural Dynamics IFASD 2019, 9-13 June 2019, Savannah, Georgia, USA, pp. 094–1, Curran, 2019.

Domino, S.: Sierra low mach module: Nalu theory manual 1.0, SAND2015-3107W, Sandia National Laboratories Unclassified Unlimited Release (UUR), 30, 2015.

Falgout, R. D. and Yang, U. M.: hypre: A library of high performance preconditioners, in: International Conference on Computational Science, pp. 632–641, Springer, https://doi.org/10.1007/3-540-47789-6_66, 2002.

Heroux, M. A., Bartlett, R. A., Howle, V. E., Hoekstra, R. J., Hu, J. J., Kolda, T. G., Lehoucq, R. B., Long, K. R., Pawlowski, R. P., Phipps, E. T., et al.: An overview of the Trilinos project, ACM Transactions on Mathematical Software (TOMS), 31, 397–423, https://doi.org/10.1145/1089014.1089021, 2005.

Jonkman, B., Mudafort, R., Platt, A., Branlard, E., Sprague, M., Jonkman, J., Hayman, G., Vijayakumar, G., Buhl, M., Ross, H., et al.: OpenFAST/openfast: OpenFAST v4.1.1, https://zenodo.org/records/15844128, 2025.

Jonkman, J.: The new modularization framework for the FAST wind turbine CAE tool, in: 51st AIAA Aerospace Sciences Meeting Including the New Horizons Forum and Aerospace Exposition, p. 202, https://doi.org/10.2514/6.2013-202, 2013.

Kuhn, M. B., Henry de Frahan, M. T., Mohan, P., Deskos, G., Churchfield, M., Cheung, L., Sharma, A., Almgren, A., Ananthan, S., Brazell, M. J., et al.: AMR-Wind: A performance-portable, high-fidelity flow solver for wind farm simulations, Wind Energy, 28, e70 010, https://doi.org/10.1002/we.70010, 2025.

Lee, B., Vijayakumar, G., and Sprague, M.: Assessment and improvement of the SST-gamma transition model in Nalu-Wind, Journal of Aircraft, pp. 1–22, https://doi.org/10.2514/1.C038368, 2025.

Menter, F. R., Kuntz, M., Langtry, R., et al.: Ten years of industrial experience with the SST turbulence model, Turbulence, Heat and Mass Transfer, 4, 625–632, 2003.

Menter, F. R., Smirnov, P. E., Liu, T., and Avancha, R.: A one-equation local correlation-based transition model, Flow, Turbulence and Combustion, 95, 583–619, https://doi.org/10.1007/s10494-015-9622-4, 2015.

https://doi.org/10.5194/wes-2025-263
Preprint. Discussion started: 21 January 2026

Mullowney, P., Li, R., Thomas, S., Ananthan, S., Sharma, A., Rood, J. S., Williams, A. B., and Sprague, M. A.: Preparing an incompressible-flow fluid dynamics code for exascale-class wind energy simulations, in: Proceedings of the International Conference for High Performance Computing, Networking, Storage and Analysis (SC21), pp. 1–16, https://doi.org/10.1145/3458817.3476185, 2021.

Riso, C. and Cesnik, C.: Geometrically nonlinear effects in wing aeroelastic dynamics at large deflections, Journal of Fluids and Structures, 120, 103 897, https://doi.org/10.1016/j.jfluidstructs.2023.103897, 2023a.

Riso, C. and Cesnik, C.: Impact of low-order modeling on aeroelastic predictions for very flexible wings, Journal of Aircraft, 60, 662–687, https://doi.org/10.2514/1.C036869, 2023b.

Ritter, M., Hilger, J., Ribeiro, A., Öngüt, A., Righi, M., Raveh, D. E., dos Santos, L. G. P., Drachinsky, A., Riso, C., Cesnik, C. E., et al.: Collaborative Pazy wing analyses for the third aeroelastic prediction workshop, in: AIAA SciTech 2024 Forum, p. 0419, https://doi.org/10.2514/6.2024-0419, 2024.

Roget, B. and Sitaraman, J.: Robust and efficient overset grid assembly for partitioned unstructured meshes, Journal of Computational Physics, 260, 1–24, https://doi.org/10.1016/j.jcp.2013.12.021, 2014.

Sharma, A., Ananthan, S., Sitaraman, J., Thomas, S., and Sprague, M. A.: Overset meshes for incompressible flows: On preserving accuracy of underlying discretizations, Journal of Computational Physics, 428, 109 987, https://doi.org/10.1016/j.jcp.2020.109987, 2021.

Sharma, A., Brazell, M. J., Vijayakumar, G., Ananthan, S., Cheung, L., deVelder, N., Henry de Frahan, M. T., Matula, N., Mullowney, P., Rood, J., et al.: ExaWind: Open-source CFD for hybrid-RANS/LES geometry-resolved wind turbine simulations in atmospheric flows, Wind Energy, 27, 225–257, https://doi.org/10.1002/we.2886, 2024.

Sprague, M. A., Ananthan, S., Vijayakumar, G., and Robinson, M.: ExaWind: A multifidelity modeling and simulation environment for wind energy, in: Journal of Physics: Conference Series, vol. 1452, p. 012071, IOP Publishing, https://doi.org/10.1088/1742-6596/1452/1/012071, 2020.

Tang, D. and Dowell, E. H.: Experimental and theoretical study on aeroelastic response of high-aspect-ratio wings, AIAA Journal, 39, 1430–1441, https://doi.org/10.2514/2.1484, 2001.

Veers, P. S., Ashwill, T. D., Sutherland, H. J., Laird, D. L., Lobitz, D. W., Griffin, D. A., Mandell, J. F., Musial, W. D., Jackson, K., Zuteck, M., et al.: Trends in the design, manufacture and evaluation of wind turbine blades, Wind Energy: An International Journal for Progress and Applications in Wind Power Conversion Technology, 6, 245–259, https://doi.org/10.1002/we.90, 2003.

Wang, Q., Sprague, M. A., Jonkman, J., Johnson, N., and Jonkman, B.: BeamDyn: a high-fidelity wind turbine blade solver in the FAST modular framework, Wind Energy, 20, 1439–1462, https://doi.org/10.1002/we.2101, 2017.